
KEEP IT LIGHT! SIMPLIFYING IMAGE CLUSTERING VIA TEXT-FREE ADAPTERS

Yicen Li^{1,2,*}, Haitz Sáez de Ocariz Borde³, Anastasis Kratsios^{1,2,†}, Paul D. McNicholas^{1,2}

¹Department of Mathematics and Statistics, McMaster University, Hamilton, Canada

²Vector Institute, Toronto, Canada

³University of Oxford, Oxford, United Kingdom

li2642@mcmaster.ca, kratsioa@mcmaster.ca

February 7, 2025

ABSTRACT

Many competitive clustering pipelines have a multi-modal design, leveraging large language models (LLMs) or other text encoders, and text-image pairs, which are often unavailable in real-world downstream applications. Additionally, such frameworks are generally complicated to train and require substantial computational resources, making widespread adoption challenging. In this work, we show that in deep clustering, competitive performance with more complex state-of-the-art methods can be achieved using a text-free and highly simplified training pipeline. In particular, our approach, Simple Clustering via Pre-trained models (SCP), trains only a small cluster head while leveraging pre-trained vision model feature representations and positive data pairs. Experiments on benchmark datasets—including CIFAR-10, CIFAR-20, CIFAR-100, STL-10, ImageNet-10, and ImageNet-Dogs—demonstrate that SCP achieves highly competitive performance. Furthermore, we provide a theoretical result explaining why, at least under ideal conditions, additional text-based embeddings may not be necessary to achieve strong clustering performance in vision.

1 Introduction

Powered by the expressive capabilities of neural networks, deep clustering (DC) has redefined the state of the art (SOTA) in image clustering, outperforming traditional algorithms by indisputable margins. These DC pipelines uncover subtle features that can significantly enhance the power of downstream learners. A highly non-exhaustive list of algorithms redefining their respective SOTA includes DC-powered methods for community detection [1, 2], anomaly detection [3], image segmentation [4, 5], object detection [6, 7], and medical applications [8]. However, many recent DC pipelines rely on *massive* models, often powered by large language models (LLMs), which may be unnecessarily compute-intensive for clustering tasks, as well as complicated training schemes. This motivates our main research question:

Is SOTA performance achievable with a simple DC pipeline? (Q1)

Indeed, we show that competitive performance, SOTA and near-SOTA, can be achieved using only a small adapter modifying the features generated by a pre-trained text-free, image encoder, i.e. not requiring any additional input text from the user, LLMs, or any other variants of text encoders. The result is a *lightweight* and *simple* end-to-end DC pipeline, which is computationally cheap enough to be run on a standard L4 GPU. Hence, our framework is easy to deploy in real-world tasks, as it is computationally accessible to most practitioners and does not require text-image pairs, which may not always be readily available in practical clustering applications.

*Corresponding author. Email: li2642@mcmaster.ca

†Corresponding author. Email: kratsioa@mcmaster.ca

1.1 Theoretical Motivation

The intuition behind why a text-free classifier should, at least theoretically, be able to match the power of a classifier using text embeddings together with the raw pixel data is rooted in our theoretical results. If X represents a random image and Z is its corresponding semantic description, which itself is a compressed representation of the information *only* in the random image X , then any classification task Y that depends on both the image X and its textual information can ultimately be expressed as a function of the image X alone. We denote the σ -algebra generated by the random variable X by $\sigma(X)$.

Proposition 1.1 (Lossless Amortization Principle (LAR)). *Fix $d, D, C \in \mathbb{N}$. Let X, Z be random variables respectively, taking values in \mathbb{R}^d and in \mathbb{R}^D , both of which are defined on a common probability space $(\Omega, \mathcal{F}, \mathbb{P})$, and suppose that Z is $\sigma(X)$ -measurable. For every $\{0, 1, \dots, C-1\}$ -valued random variable Y on $(\Omega, \mathcal{F}, \mathbb{P})$ if: there exists a Borel measurable function $f : (\mathbb{R}^{d+D}, \mathcal{B}(\mathbb{R}^{d+D})) \rightarrow (\mathbb{R}^d, \mathcal{B}(\mathbb{R}^d))$ representing Y by*

$$\underbrace{Y = f(X, Z)}_{\text{Depends both on } X \text{ and } Z} \tag{1}$$

then, there is a Borel map $F : (\mathbb{R}^d, \mathcal{B}(\mathbb{R}^d)) \rightarrow (\mathbb{R}^n, \mathcal{B}(\mathbb{R}^n))$ providing the following lossless amortized representation

$$Y = \underbrace{F(X)}_{\text{Only depends on } X} \tag{LAR}$$

Proof. See Appendix B. □

Further, the proposition above seems to align with the *Platonic Representation Hypothesis* proposed in [9], which suggests that latent representations in deep networks converge despite being trained on distinct data modalities. This supports our claim that, as long as the backbone vision model provides sufficiently good latent representations, the addition of extra modality inputs may be unnecessary.

Note that we acknowledge that, generally speaking, using multimodal representations and additional information for our networks to make predictions empirically tends to yield better results. Rather than disputing this, we aim to theorize whether, in principle and under ideal conditions, clustering could be achieved using the simplest model possible, without cumbersome multimodal data collection.

Our LAR principle (Proposition 1.1) shows that any semantically-powered image classifier may be realized by a text-free classifier “ F ”. However, *can this theoretical classifier be practically realized, at-least approximately?* Our main theoretical result guarantees that the theoretical text-free classifiers can indeed be approximately implemented by an MLP with a softmax output activation. Our guarantee holds for multiclass MLP classifiers using any standard activation function such as ReLU, Swish, or softplus.

Theorem 1.2 (Text-Free DC is Powerful Enough). *In the setting of Proposition 1.1, let $\rho : \mathbb{R} \rightarrow \mathbb{R}$ be an activation function with at least one point of continuous and non-zero differentiability. Then, for every $0 < \varepsilon \leq 1$, there is an MLP $\hat{F} : \mathbb{R}^d \rightarrow \mathbb{R}^C$, with activation function ρ , satisfying*

$$\left| \underbrace{f(X, Z)}_{\text{text-dependent classes}} - \underbrace{\text{softmax} \circ \hat{F}(X)}_{\text{text-free deep learner}} \right| < \varepsilon \tag{2}$$

with probability at least $1 - \varepsilon$.

Proof. See Appendix B. □

1.2 Simplifying Contemporary Deep Clustering

Modern clustering pipelines, e.g. [10, 11] usually involve: **(i)** learning powerful initial latent representations through self-supervised techniques, e.g. joint-embedding approaches [12, 13], and **(ii)** gradually refining the representation and clustering membership by minimizing an objective function [14].

Representation Learning in Deep Clustering The emergence of large-scale pre-trained models optimized according to a contrastive learning objective using both natural language such as CLIP [15] and purely image-based encoders like DINO [16, 17], has proven highly effective in capturing rich, general-purpose feature representations for a variety of downstream tasks. Most SOTA-achieving DC pipelines leverage these powerful representations alongside text-embedding [18, 19] (the Z in Theorem 1.2) for effective latent feature alignment. However, as we will see in Section 4,

these text-based representations seem to contain redundant features, given that similar performance can be achieved without them. As we have already mentioned, being able to eliminate the need for text would make downstream applications, particularly in data-scarce regimes, much more accessible to the end user.

Self-Supervised Training Typically, modern DC pipelines are trained using self-supervised methods by optimizing contrastive losses [20]. While contrastive methods rely on both positive and negative pairs, other approaches like BYOL [21] have demonstrated that it is possible to learn effective representations without negative pairs by simply maximizing the agreement between two views of the same data. This suggests that maximizing similarities of positive pairs alone can yield high-quality representations. We will follow a similar approach in this work too, see Section 3.

From Theory to Practice Even if the model is approximately optimal and its parameters are perfectly adjusted, it is not clear that any real-world unsupervised training procedure can achieve the theoretical expressivity guaranteed by Theorem 1.2. Hence, we would like to empirically answer whether *unimodal text-free DC pipelines can rival multimodal ones*. We would like to emphasize that obtaining powerful DC performance, with the additional requirement that our DC pipeline is simple, unimodal, and text-free, is highly nontrivial since even the current SOTA in deep clustering exhibits a *substantial* performance gap with respect to supervised image classification models. Indeed, supervised methods typically achieve accuracies well-above 90% on image datasets, while unsupervised clustering approaches rarely surpassed 50% clustering accuracy on CIFAR-20, and many fall below 50% [22, 23, 24, 25]. This is because most unsupervised clustering pipelines struggle with complex natural images due to high intra-class variability.

Contributions To address the challenges discussed so far, we propose Simple Clustering via Pre-trained models (SCP). Our main contributions are as follows:

- **Simple DC Pipeline:** Our method yields competitive results while maintaining a simple yet effective architecture, requiring no additional feature layers, support sets, teacher-student networks, text information, or exponential moving averages.
- **Text-Free (Unimodal) Encodings:** We integrate the powerful image encoder from CLIP (and also experiment with DINO) into a self-supervised clustering framework and show that this approach achieves competitive clustering performance on benchmark datasets such as CIFAR-10 [26], CIFAR-20 [26] and STL-10 [26] to current SOTA.
- **Principled Approach:** Our text-free approach is principled, based on the approximate representation result previously presented in Theorem 1.2, which guarantees that text-free embeddings are theoretically enough.

2 Related Work

In this section, we provide a broad overview of self-supervised learning research that has inspired our work, along with recent trends in image clustering using pre-trained models.

2.1 Self-Supervised Learning

Self-supervised learning learns representations from data without explicit labels. The objective is to create a representation space where positive pairs are closer together, while negative pairs are pushed farther apart [27].

SimCLR [12] uses data augmentations, such as flipping and colour jittering, to create positive and negative pairs for optimizing objectives. It also introduces a projection head that maps embeddings into a space where contrastive loss is applied. BYOL [21] shows that high-quality representations can be learned by simply maximizing agreement between two augmented views of the same input, without requiring negative pairs. Building on these advancements, SimSiam [28] eliminates the need for both negative pairs and momentum encoders by introducing a stop-gradient operation, which effectively prevents representational collapse. Inspired by these methods, we adopt similar ideas to develop a simple and effective self-supervised framework for image clustering.

2.2 Pre-trained Models in Vision

Building on advances in self-supervised learning, CLIP [15] introduced a paradigm of contrastive pre-training that aligns images with corresponding textual descriptions. This approach enables broad task generalization without task-specific fine-tuning. DINO [16], which stands for self-distillation with no labels, demonstrates a self-supervised method for optimizing a student network from a teacher network based on vision input data only.

One of the key advantages of pre-trained models like CLIP is their ability to eliminate the need for training models from scratch for downstream tasks, significantly reducing computational costs and time. Instead of training a self-supervised neural network from the ground up, pre-trained models provide high-quality feature representations out of the box, leading to faster experimentation and improved performance on a variety of tasks. The scalability of CLIP has been further validated by openCLIP [29], which extended CLIP using the larger Vision Transformer models [30]. Similarly, models such as DINO [31] and DINOv2 [17] are capable of processing visual data and mapping it to high-quality latent representations.

2.3 Image Clustering via Pre-trained Models

To address the challenges of scaling to modern image datasets, methods such as NMCE [32] and MLC [33] have integrated deep learning with manifold clustering using the minimum coding rate principle [34]. Building on this idea, CPP [35] further refines CLIP features and estimates the optimal number of clusters when unknown. TEMI [36] improves clustering by leveraging associations between image features, introducing a variant of pointwise mutual information with instance weighting. Unlike our approach, TEMI utilizes a nearest-neighbors set and an exponential moving average for parameter optimization.

SIC [19] leverages multi-modality by mapping images to a semantic space and generating pseudo-labels based on image-semantic relationships. More recently, TAC [18] utilizes the textual semantics of WordNet [37] to enhance image clustering by selecting and retrieving nouns that best distinguish the images, facilitating collaboration between text and image modalities through mutual cross-modal neighborhood distillation.

Current pre-trained approaches often rely on heavy or complex architectures to ensure consistency, motivating us to develop a simple yet effective pipeline for image clustering. Our method requires only a simple clustering head and basic data augmentations, demonstrating strong competitiveness among recent models.

3 Our Method

Recent methods such as CC [23] and CPP [35] decouple the latent space into clustering and feature spaces. TAC [18] utilizes text information, and TEMI [36] employs self-distillation networks to enhance clustering. In contrast, our approach remains simple and efficient without relying on these techniques. As shown in Fig. 1, SCP consists of only two components: a pre-trained frozen backbone for pair construction, denoted as $f(\cdot)$, and a trainable cluster head $g(\cdot)$.

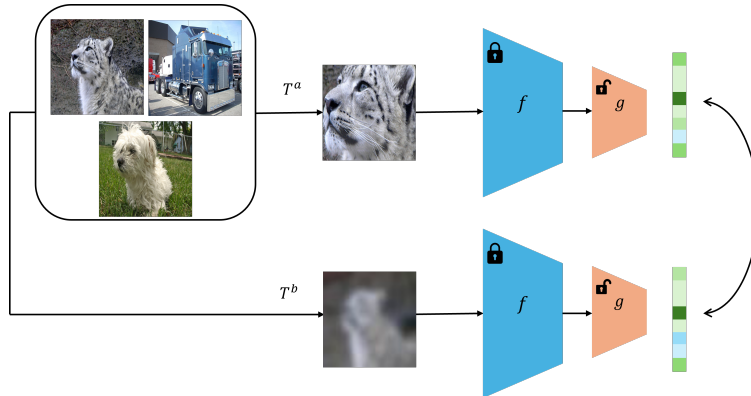


Figure 1: A overall pipeline for SCP. During training, two augmented views T^a and T^b of an image are generated from the dataset and processed by a frozen feature extractor f and a trainable cluster head g (a five-layer MLP). The objective is to minimize the cross-entropy loss between the outputs of the cluster head g for the two augmented views.

Briefly, SCP performs data augmentations and extracts features from the augmented images using pre-trained models. The cluster head then projects these features into a cluster space, where the dimension equals the number of clusters. After training, outputs in the cluster space provide the soft assignments for clustering.

3.1 Pair Construction Backbone

The success of BYOL demonstrates that we can maximize the similarities of positive pairs without negative ones. In SCP, the positive pairs consist of samples augmented from the same instance.

Given a data instance x_i , we apply two stochastic transformations T^a and T^b , independently selected from the augmentation family \mathcal{T} . This produces two correlated views: $x_i^a = T^a(x_i)$ and $x_i^b = T^b(x_i)$.

An appropriate augmentation strategy is vital for better downstream performance. In our work, we adopt only two simple augmentations: `RandomCrop` and `GaussianBlur`. This choice aligns with the preprocessing techniques used in training pre-trained models, ensuring compatibility with their learned representations. `RandomCrop` randomly crops the image to a specified size, and `GaussianBlur` applies a Gaussian filter to blur the image. For each image, these two augmentations are applied independently, each with a 50% probability. We then use a pre-trained model $f(\cdot)$, such as CLIP, to extract features from the augmented images: $h_i^a = f(x_i^a)$ and $h_i^b = f(x_i^b)$.

3.2 Cluster Head

Following the ‘‘label as representation’’ concept [23], when a data sample is projected into a space whose dimensionality matches the number of clusters K , the k -th component of its feature vector (after applying a softmax function) can be interpreted as the probability that the sample belongs to the k -th cluster. We employ a five-layer non-linear MLP as the clustering head $g(\cdot)$, producing a K -dimensional feature that is normalized with a softmax over the dimension of the cluster.

$$y_i^a = g(h_i^a), \quad y_i^b = g(h_i^b).$$

Hence, y_i^a and y_i^b are both K -dimensional vectors, whose components $y_{i,k}^a$ and $y_{i,k}^b$ indicate the probability of assigning the i -th sample to the k -th cluster. Formally, let $Y^a, Y^b \in \mathbb{R}^{N \times K}$ be the outputs of the clustering head for all samples. Then, we have the following matrices:

$$Y^a = \begin{bmatrix} y_1^a \\ \vdots \\ y_N^a \end{bmatrix}, \quad Y^b = \begin{bmatrix} y_1^b \\ \vdots \\ y_N^b \end{bmatrix}.$$

To maximize row-wise similarity, we adopt the following cross-entropy loss function instead of the commonly used InfoNCE loss [20], as SCP only have positive pairs that should share similar soft assignments:

$$L_e = - \sum_{i=1}^N \sum_{k=1}^K y_{i,k}^a \log y_{i,k}^b. \quad (3)$$

Inspired by the effective regularizations in TAC [18], we further introduce the following confidence loss to make the soft labels y_i^a and y_i^b more confident, approaching one-hot vectors:

$$L_{\text{con}} = - \log \sum_{i=1}^N y_i^{a \top} y_i^b. \quad (4)$$

This loss ensures that the cluster head assigns higher probabilities to its top predicted clusters, thereby increasing confidence in the assignments.

In addition, following TAC [18], we introduce an entropy term $H(Y)$ to prevent model collapse, defined as follows:

$$H(Y) = - \sum_{k=1}^K [P_k^a \log P_k^a + P_k^b \log P_k^b], \quad (5)$$

where

$$P_k^a = \frac{1}{N} \sum_{i=1}^N y_{i,k}^a, \quad P_k^b = \frac{1}{N} \sum_{i=1}^N y_{i,k}^b.$$

$H(Y)$ encourages uniform soft assignments across clusters, thereby mitigating the issue of empty clusters.

Hence, we define the overall objective function of SCP as

$$L_{\text{clu}} = L_e + L_{\text{con}} - \alpha H(Y), \quad (6)$$

where the balancing weight α modulates the influence of $H(Y)$, especially when the number of clusters is large. By maximizing consistency between different augmented views with regularizations, SCP effectively prevents trivial solutions and achieves competitive performance. We provide algorithm 1 to explain our pipeline.

Algorithm 1 Simple Clustering via Pre-trained Models (SCP)

Require: Dataset $\mathcal{X} = \{x_i\}_{i=1}^N$, Pre-trained model $f(\cdot)$, number of clusters K , batch size B , loss weight α

- 1: Initialize cluster head $g(\cdot)$
- 2: **for** each epoch **do**
- 3: **for** each mini-batch $\{x_i\}_{i=1}^B$ **do**
- 4: **Pair Construction:**
- 5: **for** each data instance x_i in the mini-batch **do**
- 6: Apply stochastic transformations T^a, T^b to obtain:
- 7: $x_i^a = T^a(x_i), \quad x_i^b = T^b(x_i)$
- 8: Extract features using pre-trained model:
- 9: $h_i^a = f(x_i^a), \quad h_i^b = f(x_i^b)$
- 10: **end for**
- 11: **Cluster Space Encoding:**
- 12: **for** each feature h_i^a, h_i^b **do**
- 13: Compute soft assignments: $y_i^a = g(h_i^a), \quad y_i^b = g(h_i^b)$
- 14: **end for**
- 15: **Compute Losses:**
- 16: Compute total clustering loss:
- 17: $L_{\text{clu}} = L_e + L_{\text{con}} - \alpha H(Y)$
- 18: **Update** cluster head $g(\cdot)$ parameters by minimizing L_{clu}
- 19: **end for**
- 20: **end for**
- 21: **return** soft assignments $y_i = g(h_i)$ for each $x_i \in \mathcal{X}$

4 Experiments

In this section, we evaluate the proposed SCP on six widely challenging image clustering datasets. A series of initial quantitative and qualitative comparisons, ablation studies, and hyper-parameter analyses will be carried out to investigate the effectiveness and robustness of the method.

4.1 Experimental Setup

We first introduce the datasets and metrics used for evaluation and then provide the implementation details of SCP.

4.1.1 Datasets

To evaluate the performance of SCP, we apply it to six widely used image clustering datasets: STL-10 [38], CIFAR-10 [26], CIFAR-20 [26], CIFAR-100 [26], ImageNet-10 [39], and ImageNet-Dogs [39], which is a subset from ImageNet-1k [40]. The brief information of all datasets used in our evaluation is summarized in Table 1.

Table 1: Characteristics of the benchmark datasets used in our evaluation.

DATASET	SPLIT (TRAIN/TEST)	# TRAINING	# TESTING	# CLASSES
STL-10	TRAIN/TEST	5,000	8,000	10
CIFAR-10	TRAIN/TEST	50,000	10,000	10
CIFAR-20	TRAIN/TEST	50,000	10,000	20
CIFAR-100	TRAIN/TEST	50,000	10,000	100
IMAGENET-10	TRAIN/VAL	13,000	500	10
IMAGENET-DOGS	TRAIN/VAL	19,500	750	15

4.1.2 Implementation Details

In most experiments, we utilized the CLIP [15] with the backbone ViT-B/32 [30]. For a fair comparison with TEMI [36] and CPP [35], we replaced the CLIP backbone with ViT-L/14 to match the architectures used in these methods. The cluster head g is a five-layer MLP with dimensions: $D \rightarrow 1024 \rightarrow 786 \rightarrow 512 \rightarrow 1024 \rightarrow K$, where D denotes the output dimension of the pre-trained model and K represents the number of clusters.

We train the model using the Adam optimizer with a cosine annealing learning rate schedule, starting from an initial rate of 1×10^{-3} for 30 epochs. The batch size is set to 512 for all datasets. For regularization, we set $\alpha = 2$ for CIFAR-20 and ImageNet-Dogs, $\alpha = 3$ for CIFAR-100 to account for its larger number of clusters, and $\alpha = 1$ for the remaining datasets. All experiments are conducted on a single NVIDIA L4 GPU. Under this setup, training SCP on CIFAR-10 takes approximately one minute, excluding data augmentation.

4.2 Main Results

We compare our method with state-of-the-art baselines on six widely-used image clustering datasets, with feature visualizations to show the competitiveness of our proposed SCP.

4.2.1 Comparison against classical and text-based methods

We first evaluate our pipeline on five widely used datasets and compare it with 18 deep clustering baselines. Since most earlier baselines adopt ResNet-34 or ResNet-18 as the backbone, we mainly focus on comparisons with CLIP and CLIP-based methods. Specifically, CLIP (zero-shot) uses CLIP’s pre-trained image and text encoders to classify images by matching them to text prompts, while CLIP (K-means) clusters directly on CLIP image features via K-means. Our approach includes SCP-CLIP, which employs a ViT-B/32 backbone like other CLIP-based methods, and SCP-DINO, which uses a ViT-B/8 backbone. Each experiment is repeated 50 times, and the best results are reported.

Table 2: Clustering performance of various baseline methods on multiple datasets (all metrics are multiplied by 100). We highlight the best and second-best results in **boldfaced red** and **underlined in blue**, respectively. CLIP (K-means), CLIP (zero-shot), SCP-CLIP, SIC, and TAC **all adopt a ViT-B/32 backbone**. SCP-DINO uses a **ViT-B/8 backbone**.

METHOD	TEXT-FREE	STL-10			CIFAR-10			CIFAR-20			IMAGENET-10			IMAGENET-DOGS		
		NMI	ACC	ARI	NMI	ACC	ARI									
JULE [41]	✓	18.2	27.7	16.4	19.2	27.2	13.8	10.3	13.7	3.3	17.5	30.0	13.8	5.4	13.8	2.8
DEC [42]	✓	27.6	35.9	18.6	25.7	30.1	16.1	13.6	18.5	5.0	28.2	38.1	20.3	12.2	19.5	7.9
DAC [39]	✓	36.6	47.0	25.7	39.6	52.2	30.6	18.5	23.8	8.8	39.4	52.7	30.2	21.9	27.5	11.1
DCCM [43]	✓	37.6	48.2	26.2	49.6	62.3	40.8	28.5	32.7	17.3	60.8	71.0	55.5	32.1	38.3	18.2
IIC [44]	✓	49.6	59.6	39.7	51.3	61.7	41.1	22.5	25.7	11.7	-	-	-	-	-	-
PICA [45]	✓	61.1	71.3	53.1	59.1	69.6	51.2	31.0	33.7	17.1	80.2	87.0	76.1	35.2	35.3	20.1
CC [23]	✓	76.4	85.0	72.6	70.5	79.0	63.7	43.1	42.9	26.6	85.9	89.3	82.2	44.5	42.9	27.4
IDFD [46]	✓	64.3	75.6	57.5	71.1	81.5	66.3	42.6	42.5	26.4	89.8	95.4	90.1	54.6	59.1	41.3
SCAN [10]	✓	69.8	80.9	64.6	79.7	88.3	77.2	48.6	50.7	33.3	-	-	-	61.2	59.3	45.7
MICE [47]	✓	63.5	75.2	57.5	73.7	83.5	69.8	43.6	44.0	28.0	-	-	-	42.3	43.9	28.6
GCC [48]	✓	68.4	78.8	63.1	76.4	85.6	72.8	47.2	47.2	30.5	84.2	90.1	82.2	49.0	52.6	36.2
NNM [22]	✓	66.3	76.8	59.6	73.7	83.7	69.4	48.0	45.9	30.2	-	-	-	60.4	58.6	44.9
TCC [24]	✓	73.2	81.4	68.9	79.0	90.6	73.3	47.9	49.1	31.2	84.8	89.7	82.5	55.4	59.5	41.7
SPICE [25]	✓	81.7	90.8	81.2	73.4	83.8	70.5	44.8	46.8	29.4	82.8	92.1	83.6	57.2	64.6	47.9
SIC [19]		95.3	98.1	95.9	84.7	92.6	84.4	59.3	58.3	43.9	97.0	98.2	96.1	69.0	69.7	55.8
TAC [18]		95.5	98.2	96.1	83.3	91.9	83.1	61.1	60.7	44.8	98.5	99.2	98.3	80.6	83.0	72.2
SCP-CLIP	✓	94.6	97.9	95.1	85.5	93.2	85.7	59.5	60.1	44.3	97.4	98.5	97.9	56.3	59.6	44.6
SCP-DINO	✓	95.8	98.4	96.5	89.2	95.2	89.8	58.9	59.3	42.8	95.9	98.8	96.7	77.1	80.5	70.5
CLIP (K-MEANS)	✓	92.2	94.5	89.5	71.3	75.2	62.6	50.8	48.1	30.6	96.9	98.2	96.1	39.8	38.1	20.1
CLIP (ZERO-SHOT)		93.9	97.1	93.7	80.7	90.0	79.3	55.3	58.3	39.8	95.8	97.6	94.9	73.5	72.8	58.2

As shown in Table 2, our method significantly enhances clustering performance across multiple benchmark datasets. For example, on CIFAR-10, CLIP (K-means) achieves an ACC of 75.2%, whereas SCP-CLIP improves this by 18%, surpassing TAC by 1.3%. On CIFAR-20, SCP-CLIP attains an ACC of 60.1%, outperforming SIC by 1.8%. Moreover, SCP-DINO boosts performance on four benchmarks, achieving state-of-the-art results on STL-10 and the second-best performance on both ImageNet-10 and ImageNet-Dogs. The lower performance of SCP-CLIP on ImageNet-Dogs may stem from the difficulty of capturing discriminative features in fine-grained images, particularly without aligned text features.

Notably, SCP relies exclusively on visual features but still surpasses CLIP zero-shot on all benchmarks and outperforms TAC on both STL-10 and CIFAR-10. Results underscore its effectiveness in extracting and leveraging visual information for clustering. Furthermore, our pipeline is text-free, featuring a simpler architecture with fewer hyperparameters—making it especially advantageous for adaptation to pure visual pre-trained models.

Overall, these results demonstrate that beyond zero-shot classification or multi-modal frameworks, a simpler approach can still effectively utilize the power of pre-trained models for image clustering.

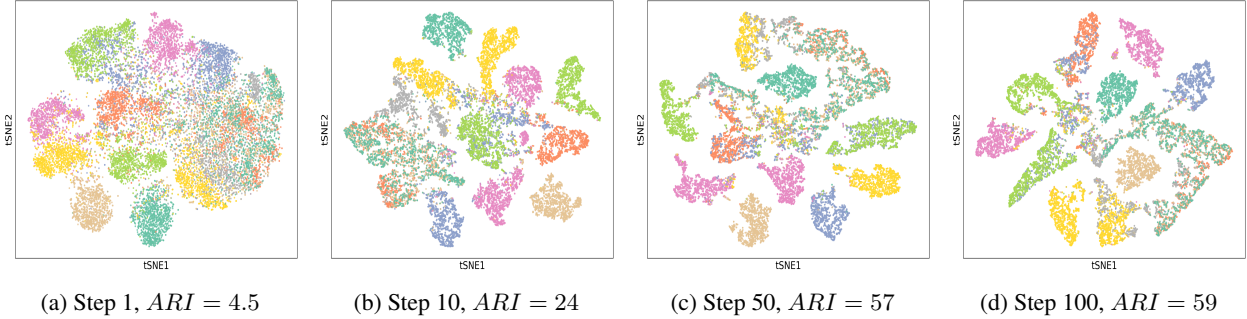


Figure 2: Visualization of representations from different training steps learned by SCP-DINO on the ImageNet-Dogs training set, along with the corresponding clustering ARI (multiplied by 100). (a) Image embeddings directly from the DINO image encoder, with clusters obtained using K-means. (b)–(d) Image logits learned by SCP-DINO across different steps. There are 77 steps per epoch.

4.2.2 Comparison with recent text-free methods

To supplement our answers to Question (Q1), we introduce SCP-MIX, which leverages the concatenated visual features from both CLIP and DINO. Alongside SCP-CLIP, we compare this method against two recent text-free approaches, TEMI [36] and CPP [35], as reported in Table 3.

Table 3: Clustering performance comparison for recent text-free methods. The best and second-best results are highlighted in **boldface red** and underlined in blue, respectively. All methods use the ViT-L/14 backbone, and SCP-MIX adopts the concatenation (or ensemble) of features learned by CLIP (ViT-L/14) and DINO (ViT-B/8).

METHOD	TEXT-FREE	CIFAR-10		CIFAR-20		CIFAR-100	
		NMI	ACC	NMI	ACC	NMI	ACC
TEMI [36]	✓	92.6	96.9	64.5	61.8	79.9	73.7
CPP [35]	✓	<u>93.6</u>	97.4	<u>72.5</u>	64.2	81.8	<u>74.0</u>
SCP-CLIP	✓	<u>93.6</u>	<u>97.5</u>	69.2	<u>65.8</u>	80.1	74.1
SCP-MIX	✓	95.0	98.0	72.9	67.5	<u>80.3</u>	73.8

SCP-MIX outperforms CPP and TEMI on both CIFAR-10 and CIFAR-20, while SCP-CLIP achieves the highest accuracy on CIFAR-100. These results underscore the competitive performance of SCP, highlighting effectiveness and simplicity. Notably, SCP achieves these outcomes without relying on additional feature layers, support sets, self-distillation, or exponential moving average strategies. Thus, unimodal text-free deep clustering method can rival multimodal pipelines.

4.3 Visualization

To provide an intuitive understanding of the clustering results, we visualize the clustering performance obtained from SCP in Fig. 3, along with learned representations on the CIFAR-10 dataset in Fig. 4. The image logits, representing SCP outputs before the final softmax function, are used for visualization, with t-SNE applied to reduce the feature dimensions. As shown, compared to embeddings directly learned by pre-trained models, SCP effectively forms well-separated clusters, leading to a higher ACC score. Without aligned text, SCP successfully extracts image features by incorporating a clustering head, resulting in superior within-cluster compactness and between-cluster separability. The visualization supports our quantitative results and highlights SCP’s effectiveness in learning discriminative features suitable for lightweight clustering tasks. Furthermore, Fig. 2 demonstrates that SCP requires only a few steps to establish a clustering structure, effectively separating certain image embeddings within 100 steps. For instance, from step 10 to step 50, SCP learns to push the light-green cluster away from the blue cluster.

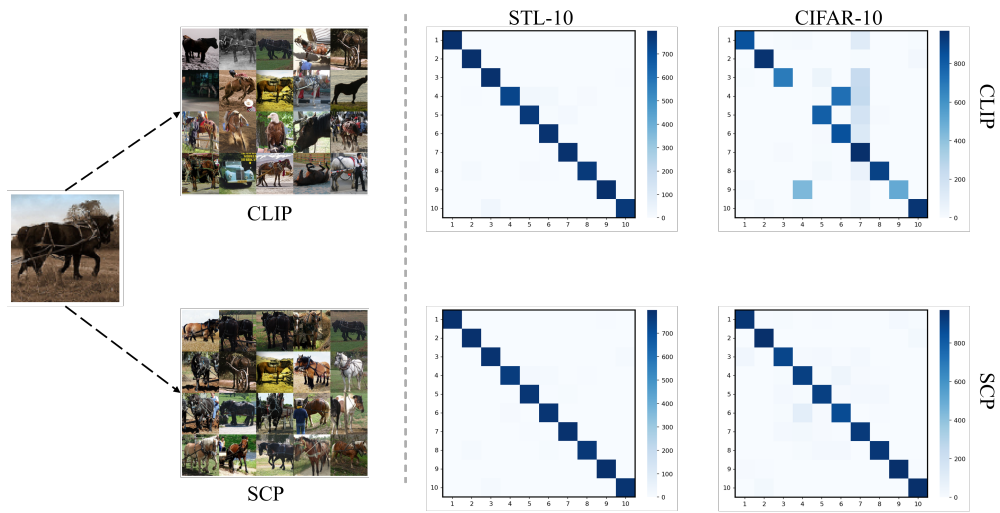


Figure 3: The visualization of clustering performance for SCP-CLIP with **ViT-B/32 backbone**. (Left): An example of an image-to-image search on STL-10, showing clusters produced by CLIP (Top) and SCP (Bottom); (Right): Visualization of clustering performance. SCP-CLIP effectively enhances CLIP’s clustering performance through a cluster head.

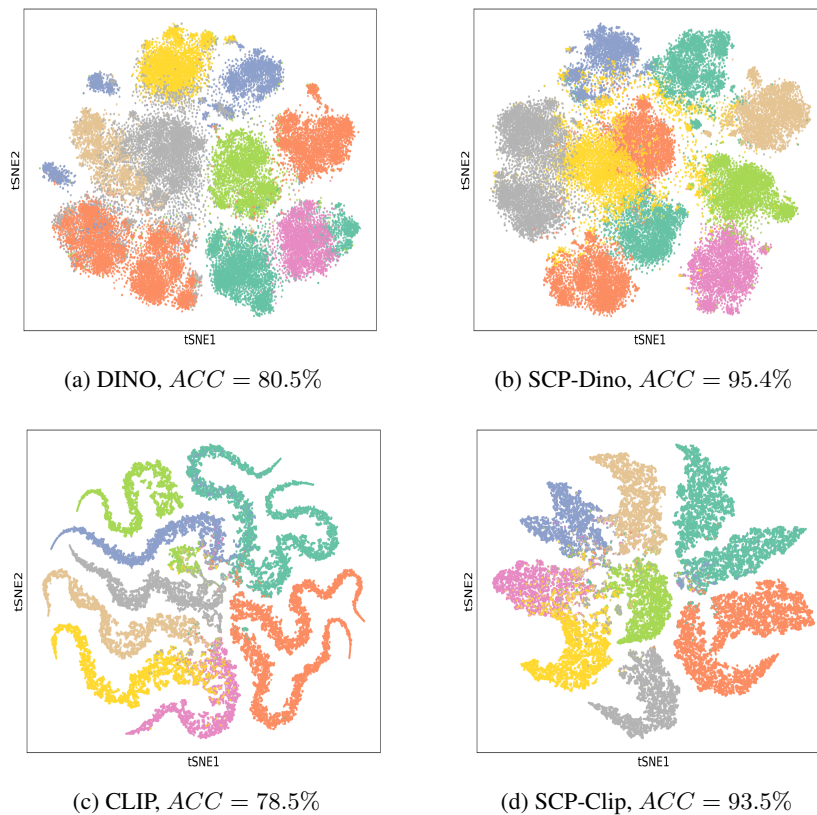


Figure 4: Visualization of representations learned by different methods on the CIFAR-10 training set, along with the corresponding clustering accuracy (ACC). (a) Image embeddings directly from the DINO image encoder, with clusters obtained by K-means. (b) Image logits from SCP-DINO. (c) Image embeddings directly from the CLIP image encoder, again clustered by K-means. (d) Image logits from SCP-CLIP.

4.4 Ablation Studies

To assess the effectiveness of the three loss terms, L_e , L_{con} , and $H(Y)$, we evaluate the performance of SCP using different combinations of these losses, as presented in Table 4. The results reveal several important insights: i) $H(Y)$ plays a crucial role in preventing cluster collapse. Without $H(Y)$, SCP tends to assign most images to only a few clusters, resulting in the model collapse on CIFAR-10 and CIFAR-20. ii) L_{con} provides a slight boost in performance. The reason is that the cluster assignments would be less confident when the cluster number increases. iii) The combination of all losses effectively learns image information, leading to the best clustering performance in this table.

Table 4: Clustering results for different losses on CIFAR-10 and CIFAR-20. A '-' indicates model collapse.

L_E	L_{CON}	$H(Y)$	CIFAR-10			CIFAR-20		
			NMI	ACC	ARI	NMI	ACC	ARI
✓			-	-	-	-	-	-
✓	✓		-	-	-	-	-	-
✓	✓	✓	85.5	93.2	85.7	59.5	60.1	44.3
	✓		-	-	-	-	-	-
	✓	✓	83.0	90.4	81.4	<u>55.7</u>	<u>53.1</u>	<u>37.6</u>
		✓	16.0	22.6	6.5	16.0	16.5	4.6
✓		✓	<u>83.9</u>	<u>91.8</u>	<u>82.9</u>	54.7	52.9	37.0

4.5 Parameter Analyses

To show how the scale of $H(Y)$ influences the performance of SCP, we evaluate it under various choices of α on training sets of CIFAR-10, CIFAR-20, CIFAR-100 and ImageNet-Dogs under 5 random seeds. The average results and the corresponding standard deviations are presented in Fig. 5.

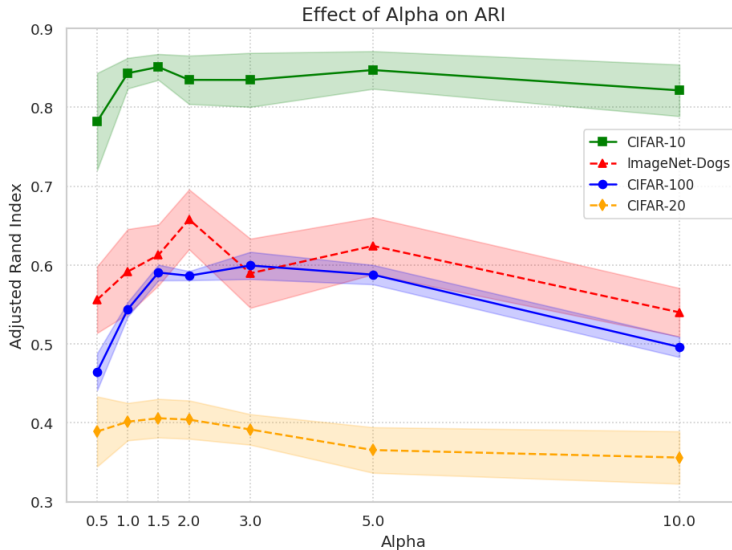


Figure 5: Comparison of different loss weights α , the solid line is the mean ARI across five runs, and the shaded region plots the standard deviation across our runs.

We observe that setting the loss weight α too low (e.g., below 0.5) makes it difficult for our method to converge. For CIFAR-10, the performance remains relatively stable and is not sensitive to large α values. In contrast, for ImageNet-dogs and CIFAR-20, choosing $\alpha = 2$ leads to better results, suggesting it provides an optimal balance between regularization and scale. For CIFAR-100, which involves a larger number of clusters, a higher α value is more suitable. Based on these findings, we select $\alpha = 3$ for CIFAR-100, $\alpha = 2$ for CIFAR-20 and ImageNet-dogs, and $\alpha = 1$ for all other datasets. It is also consistent with the prior knowledge of the number of clusters in each dataset.

5 Conclusion

In this work, we set out to determine whether a simple DC pipeline could achieve the performance of other recent clustering frameworks. Specifically, we aimed to achieve this without relying on text, as we argue that doing so would make image-based clustering much more practical for downstream applications. This is because image-pair datasets are highly unlikely to be readily available to practitioners for most real-world use cases. Moreover, we aimed to develop a method that is simple to train without the need for additional feature layers, support sets, teacher-student networks, or exponential moving averages.

To meet this desiderata we proposed SCP, a novel, simple, and lightweight clustering method that achieves SOTA and near-SOTA performance in several datasets such as STL-10, CIFAR-10, CIFAR-20, ImageNet-10, and ImageNet-Dogs. In particular, SCP leverages pre-trained CLIP and DINO backbones, and we anticipate these could be updated in the future with better models, or ensembles.

Limitations Despite these promising results, several challenges remain. Firstly, our pipeline relies on data augmentations, which can be time-consuming when scaling to larger datasets such as ImageNet-1K. Also, our approach requires prior knowledge of the number of clusters, which can be difficult to determine in practical applications unless the practitioner poses strong domain knowledge. Lastly, our frameworks performance is bounded by the quality of the pre-trained model used. However, we anticipate these to continue to improve in the future.

Impact Statement

This paper presents work whose goal is to advance the field of Machine Learning. There are many potential societal consequences of our work, none which we feel must be specifically highlighted here.

References

- [1] Hossein Saeedi Emadi and Sayyed Majid Mazinani. A novel anomaly detection algorithm using dbscan and svm in wireless sensor networks. *Wireless Personal Communications*, 98:2025–2035, 2018.
- [2] Grigory Yaroslavtsev and Adithya Vadapalli. Massively parallel algorithms and hardness for single-linkage clustering under ℓ_p -distances. In *35th International Conference on Machine Learning (ICML’18)*, 2018.
- [3] Guansong Pang, Chunhua Shen, Longbing Cao, and Anton Van Den Hengel. Deep learning for anomaly detection: A review. *ACM computing surveys (CSUR)*, 54(2):1–38, 2021.
- [4] Shervin Minaee, Yuri Boykov, Fatih Porikli, Antonio Plaza, Nasser Kehtarnavaz, and Demetri Terzopoulos. Image segmentation using deep learning: A survey. *IEEE transactions on pattern analysis and machine intelligence*, 44(7):3523–3542, 2021.
- [5] James Liang, Tianfei Zhou, Dongfang Liu, and Wenguan Wang. Clustseg: Clustering for universal segmentation, 2023. URL <https://arxiv.org/abs/2305.02187>.
- [6] Zhong-Qiu Zhao, Peng Zheng, Shou-tao Xu, and Xindong Wu. Object detection with deep learning: A review. *IEEE transactions on neural networks and learning systems*, 30(11):3212–3232, 2019.
- [7] Chung Min Kim, Mingxuan Wu, Justin Kerr, Ken Goldberg, Matthew Tancik, and Angjoo Kanazawa. Garfield: Group anything with radiance fields, 2024. URL <https://arxiv.org/abs/2401.09419>.
- [8] Zijuan Zhao, Juanjuan Zhao, Kai Song, Akbar Hussain, Qianqian Du, Yunyun Dong, Jihua Liu, and Xiaotang Yang. Joint dbn and fuzzy c-means unsupervised deep clustering for lung cancer patient stratification. *Engineering Applications of Artificial Intelligence*, 91:103571, 2020.
- [9] Minyoung Huh, Brian Cheung, Tongzhou Wang, and Phillip Isola. Position: The platonic representation hypothesis. In Ruslan Salakhutdinov, Zico Kolter, Katherine Heller, Adrian Weller, Nuria Oliver, Jonathan Scarlett, and Felix Berkenkamp, editors, *Proceedings of the 41st International Conference on Machine Learning*, volume 235 of *Proceedings of Machine Learning Research*, pages 20617–20642. PMLR, 21–27 Jul 2024. URL <https://proceedings.mlr.press/v235/huh24a.html>.
- [10] Wouter Van Gansbeke, Simon Vandenhende, Stamatios Georgoulis, Marc Proesmans, and Luc Van Gool. Scan: Learning to classify images without labels. In *European conference on computer vision*, pages 268–285. Springer, 2020.
- [11] Tianjiao Ding, Shengbang Tong, Kwan Ho Ryan Chan, Xili Dai, Yi Ma, and Benjamin D Haeffele. Unsupervised manifold linearizing and clustering. In *Proceedings of the IEEE/CVF International Conference on Computer Vision*, pages 5450–5461, 2023.
- [12] Ting Chen, Simon Kornblith, Mohammad Norouzi, and Geoffrey Hinton. A simple framework for contrastive learning of visual representations. In *International conference on machine learning*, pages 1597–1607. PMLR, 2020.
- [13] Kaiming He, Haoqi Fan, Yuxin Wu, Saining Xie, and Ross Girshick. Momentum contrast for unsupervised visual representation learning. In *Proceedings of the IEEE/CVF conference on computer vision and pattern recognition*, pages 9729–9738, 2020.
- [14] Mathilde Caron, Piotr Bojanowski, Armand Joulin, and Matthijs Douze. Deep clustering for unsupervised learning of visual features, 2019. URL <https://arxiv.org/abs/1807.05520>.
- [15] Alec Radford, Jong Wook Kim, Chris Hallacy, Aditya Ramesh, Gabriel Goh, Sandhini Agarwal, Girish Sastry, Amanda Askell, Pamela Mishkin, Jack Clark, et al. Learning transferable visual models from natural language supervision. In *International conference on machine learning*, pages 8748–8763. PMLR, 2021.
- [16] Mathilde Caron, Hugo Touvron, Ishan Misra, Hervé Jégou, Julien Mairal, Piotr Bojanowski, and Armand Joulin. Emerging properties in self-supervised vision transformers. In *Proceedings of the IEEE/CVF international conference on computer vision*, pages 9650–9660, 2021.
- [17] Maxime Oquab, Timothée Darcet, Théo Moutakanni, Huy Vo, Marc Szafraniec, Vasil Khalidov, Pierre Fernandez, Daniel Haziza, Francisco Massa, Alaaeldin El-Nouby, Mahmoud Assran, Nicolas Ballas, Wojciech Galuba, Russell Howes, Po-Yao Huang, Shang-Wen Li, Ishan Misra, Michael Rabbat, Vasu Sharma, Gabriel Synnaeve,

- Hu Xu, Hervé Jegou, Julien Mairal, Patrick Labatut, Armand Joulin, and Piotr Bojanowski. Dinov2: Learning robust visual features without supervision, 2024. URL <https://arxiv.org/abs/2304.07193>.
- [18] Yunfan Li, Peng Hu, Dezhong Peng, Jiancheng Lv, Jianping Fan, and Xi Peng. Image clustering with external guidance. *arXiv preprint arXiv:2310.11989*, 2023.
- [19] Shaotian Cai, Liping Qiu, Xiaojun Chen, Qin Zhang, and Longteng Chen. Semantic-enhanced image clustering. In *Proceedings of the AAAI conference on artificial intelligence*, volume 37, pages 6869–6878, 2023.
- [20] Aaron van den Oord, Yazhe Li, and Oriol Vinyals. Representation learning with contrastive predictive coding. *arXiv preprint arXiv:1807.03748*, 2018.
- [21] Jean-Bastien Grill, Florian Strub, Florent Altché, Corentin Tallec, Pierre Richemond, Elena Buchatskaya, Carl Doersch, Bernardo Avila Pires, Zhaohan Guo, Mohammad Gheshlaghi Azar, et al. Bootstrap your own latent—a new approach to self-supervised learning. *Advances in neural information processing systems*, 33:21271–21284, 2020.
- [22] Zhiyuan Dang, Cheng Deng, Xu Yang, Kun Wei, and Heng Huang. Nearest neighbor matching for deep clustering. In *Proceedings of the IEEE/CVF conference on computer vision and pattern recognition*, pages 13693–13702, 2021.
- [23] Yunfan Li, Peng Hu, Zitao Liu, Dezhong Peng, Joey Tianyi Zhou, and Xi Peng. Contrastive clustering. In *Proceedings of the AAAI conference on artificial intelligence*, volume 35, pages 8547–8555, 2021.
- [24] Yuming Shen, Ziyi Shen, Menghan Wang, Jie Qin, Philip Torr, and Ling Shao. You never cluster alone. *Advances in Neural Information Processing Systems*, 34:27734–27746, 2021.
- [25] Chuang Niu, Hongming Shan, and Ge Wang. Spice: Semantic pseudo-labeling for image clustering. *IEEE Transactions on Image Processing*, 31:7264–7278, 2022.
- [26] Alex Krizhevsky, Geoffrey Hinton, et al. Learning multiple layers of features from tiny images. 2009.
- [27] Jonas Geiping, Quentin Garrido, Pierre Fernandez, Amir Bar, Hamed Pirsiavash, Yann LeCun, and Micah Goldblum. A cookbook of self-supervised learning. *arXiv preprint arXiv:2304.12210*, 2023.
- [28] Xinlei Chen and Kaiming He. Exploring simple siamese representation learning, 2020. URL <https://arxiv.org/abs/2011.10566>.
- [29] Mehdi Cherti, Romain Beaumont, Ross Wightman, Mitchell Wortsman, Gabriel Ilharco, Cade Gordon, Christoph Schuhmann, Ludwig Schmidt, and Jenia Jitsev. Reproducible scaling laws for contrastive language-image learning. In *2023 IEEE/CVF Conference on Computer Vision and Pattern Recognition (CVPR)*. IEEE, June 2023. doi:10.1109/cvpr52729.2023.00276. URL <http://dx.doi.org/10.1109/CVPR52729.2023.00276>.
- [30] Alexey Dosovitskiy. An image is worth 16x16 words: Transformers for image recognition at scale. *arXiv preprint arXiv:2010.11929*, 2020.
- [31] Mathilde Caron, Hugo Touvron, Ishan Misra, Hervé Jegou, Julien Mairal, Piotr Bojanowski, and Armand Joulin. Emerging properties in self-supervised vision transformers. In *2021 IEEE/CVF International Conference on Computer Vision (ICCV)*, pages 9630–9640, 2021. doi:10.1109/ICCV48922.2021.00951.
- [32] Zengyi Li, Yubei Chen, Yann LeCun, and Friedrich T Sommer. Neural manifold clustering and embedding. *arXiv preprint arXiv:2201.10000*, 2022.
- [33] Hua Deng, Meng Ding, Yimeng Wang, Weihua Li, Guixia Liu, and Yun Tang. Acp-mlc: a two-level prediction engine for identification of anticancer peptides and multi-label classification of their functional types. *Computers in Biology and Medicine*, 158:106844, 2023.
- [34] David Arthur and Sergei Vassilvitskii. k-means++: the advantages of careful seeding. *Symposium on Discrete Algorithms, Symposium on Discrete Algorithms*, Jan 2007.
- [35] Tianzhe Chu Chu, Shengbang Tong, Tianjiao Ding, Xili Dai, Benjamin Haeffele, Rene Vidal, and Yi Ma. Image clustering via the principle of rate reduction in the age of pretrained models. *International Conference on Learning Representations (ICLR)*, 2024.
- [36] Nikolas Adaloglou, Felix Michels, Hamza Kalisch, and Markus Kollmann. Exploring the limits of deep image clustering using pretrained models. *arXiv preprint arXiv:2303.17896*, 2023.
- [37] George A Miller. Wordnet: a lexical database for english. *Communications of the ACM*, 38(11):39–41, 1995.
- [38] Adam Coates, Andrew Ng, and Honglak Lee. An analysis of single-layer networks in unsupervised feature learning. In *Proceedings of the fourteenth international conference on artificial intelligence and statistics*, pages 215–223. JMLR Workshop and Conference Proceedings, 2011.

- [39] Jianlong Chang, Lingfeng Wang, Gaofeng Meng, Shiming Xiang, and Chunhong Pan. Deep adaptive image clustering. In *Proceedings of the IEEE international conference on computer vision*, pages 5879–5887, 2017.
- [40] Jia Deng, Wei Dong, Richard Socher, Li-Jia Li, Kai Li, and Li Fei-Fei. Imagenet: A large-scale hierarchical image database. In *2009 IEEE conference on computer vision and pattern recognition*, pages 248–255. Ieee, 2009.
- [41] Jianwei Yang, Devi Parikh, and Dhruv Batra. Joint unsupervised learning of deep representations and image clusters, 2016. URL <https://arxiv.org/abs/1604.03628>.
- [42] Junyuan Xie, Ross Girshick, and Ali Farhadi. Unsupervised deep embedding for clustering analysis, 2016. URL <https://arxiv.org/abs/1511.06335>.
- [43] Jianlong Wu, Keyu Long, Fei Wang, Chen Qian, Cheng Li, Zhouchen Lin, and Hongbin Zha. Deep comprehensive correlation mining for image clustering, 2019. URL <https://arxiv.org/abs/1904.06925>.
- [44] Xu Ji, João F. Henriques, and Andrea Vedaldi. Invariant information clustering for unsupervised image classification and segmentation, 2019. URL <https://arxiv.org/abs/1807.06653>.
- [45] Jiabo Huang, Shaogang Gong, and Xiatian Zhu. Deep semantic clustering by partition confidence maximisation. In *Proceedings of the IEEE/CVF conference on computer vision and pattern recognition*, pages 8849–8858, 2020.
- [46] Yaling Tao, Kentaro Takagi, and Kouta Nakata. Clustering-friendly representation learning via instance discrimination and feature decorrelation, 2021. URL <https://arxiv.org/abs/2106.00131>.
- [47] Tsung Wei Tsai, Chongxuan Li, and Jun Zhu. Mice: Mixture of contrastive experts for unsupervised image clustering. In *International conference on learning representations*, 2020.
- [48] Huasong Zhong, Jianlong Wu, Chong Chen, Jianqiang Huang, Minghua Deng, Liqiang Nie, Zhouchen Lin, and Xian-Sheng Hua. Graph contrastive clustering. In *Proceedings of the IEEE/CVF international conference on computer vision*, pages 9224–9233, 2021.
- [49] Olav Kallenberg. *Foundations of modern probability*, volume 99 of *Probability Theory and Stochastic Modelling*. Springer, Cham, third edition, 2021. ISBN 978-3-030-61871-1; 978-3-030-61870-4. doi:10.1007/978-3-030-61871-1. URL <https://doi.org/10.1007/978-3-030-61871-1>.
- [50] Achim Klenke. *Probability theory—a comprehensive course*. Universitext. Springer, Cham, third edition, 2020. ISBN 978-3-030-56402-5; 978-3-030-56401-8. doi:10.1007/978-3-030-56402-5. URL <https://doi.org/10.1007/978-3-030-56402-5>.
- [51] Anastasis Kratsios and Léonie Papon. Universal approximation theorems for differentiable geometric deep learning. *J. Mach. Learn. Res.*, 23:Paper No. [196], 73, 2022. ISSN 1532-4435,1533-7928.
- [52] Patrick Kidger and Terry Lyons. Universal approximation with deep narrow networks. In *Conference on learning theory*, pages 2306–2327. PMLR, 2020.

A Additional Experiment Details

A.1 Image Search Pipeline

A.1.1 CLIP for Image search

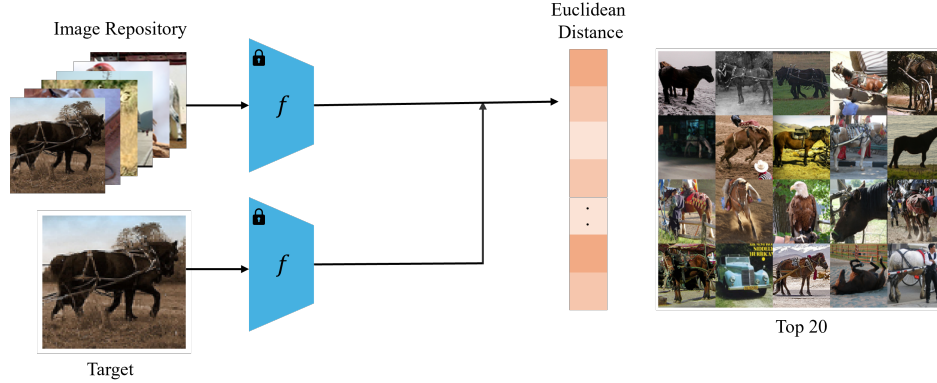


Figure 6: CLIP Image-to-Image Search baseline depicted in Fig. 3.

Figure 6 illustrates the CLIP baseline for image-to-image search. The image repository comprises the STL-10 test split, with a target image randomly selected for the search. The search process ranks images based on Euclidean distances, displaying the top 20 most similar results. The results indicate that CLIP effectively learns discriminative features, although two mismatched images are still present in the top-20 neighborhood.

A.1.2 SCP for Image search

Figure 7 illustrates the SCP-CLIP approach for image-to-image search. SCP-CLIP successfully retrieves images from the same cluster within the top-20 neighborhood.

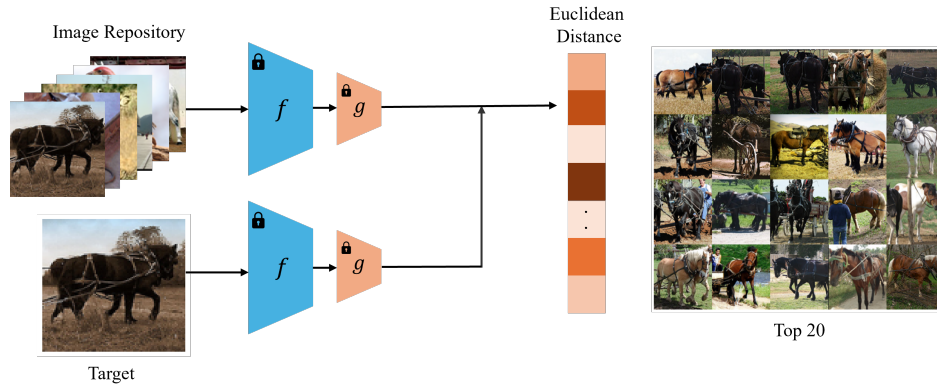


Figure 7: SCP-CLIP Image-to-Image Search Pipeline depicted in Fig. 3, utilizing the normalized outputs of the trained cluster head $g(\cdot)$ without applying softmax.

A.2 Visualization

We create a t-SNE visualization image cloud of STL-10 test set to support SCP effectiveness further. It was observed that both SCP-DINO and SCP-CLIP successfully distinguished most planes, ships, horses, and deer, even when they share a blue background or similar body shape.



Figure 8: The t-SNE representations learned by SCP-DINO on STL-10. $ACC : 98.4\%$



Figure 9: The t-SNE representations learned by SCP-CLIP on STL-10. $ACC : 97.9\%$

B Proofs

Proof of Proposition 1.1. By the Doob-Dyknin lemma, see e.g. [49, Lemma 1.14], since Z is $\sigma(X)$ -measurable if and only if there exists some Borel measurable function $g : (\mathbb{R}^d, \mathcal{B}(\mathbb{R}^d)) \rightarrow (\mathbb{R}^D, \mathcal{B}(\mathbb{R}^D))$ such that

$$Z = g(X). \quad (7)$$

Now, define $F : (\mathbb{R}^d, \mathcal{B}(\mathbb{R}^d)) \rightarrow (\mathbb{R}^n, \mathcal{B}(\mathbb{R}^n))$ by composition, as sending every $x \in \mathbb{R}^d$ to

$$F(x) \stackrel{\text{def}}{=} f(x, g(x)). \quad (8)$$

Then, together (7), the definition of Y in (1), and that of F in (8) yield

$$Y = f(X, Z) = f(X, g(X)) = F(X) \quad (9)$$

which establishes our claim. \square

Proof of Theorem 1.2. The law of X , namely the pushforward of \mathbb{P} by X denoted here by $\mu \stackrel{\text{def}}{=} X_{\#}\mathbb{P}$, is a Borel probability measure. Therefore, [50, Theorem 13.6] implies that μ is a Radon measure. Since, in addition, \mathbb{R}^d is a second-countable and locally-compact topological space then, the version of Lusin's Theorem found in [50, Exercise 13.1.3], applies. Whereby, we deduce that for every $\varepsilon \in (0, 1]$ there exists a compact subset \mathcal{K}_ε of \mathbb{R}^d satisfying

$$\mu(\mathcal{K}_\varepsilon) \geq 1 - \varepsilon \quad (10)$$

and for which the restriction of the Borel measurable map F to \mathcal{K}_ε is continuous.

Now, fix a continuous activation function $\rho : \mathbb{R} \rightarrow \mathbb{R}$ with at least one point of continuous non-zero differentiability; i.e. satisfying [51, Assumption 1] (due to [52]). As shown in [51, Example 13], the softmax function satisfies [51, Assumption 8]; whence the general case of the non-Euclidean universal approximation theorem [51, Theorem 37 (ii)] applies; from which we deduce the existence of an MLP $\hat{F} : \mathbb{R}^d \rightarrow \mathbb{R}^C$ with ρ activation function satisfying the uniform approximation guarantee

$$\sup_{x \in \mathcal{K}_\varepsilon} |F(x) - \text{softmax} \circ \hat{F}(x)| < \varepsilon. \quad (11)$$

Define the failure set

$$B \stackrel{\text{def}}{=} \left\{ x \in \mathbb{R}^d : |F(x) - \text{softmax} \circ \hat{F}(x)| \geq \varepsilon \right\}.$$

By construction, $\mathcal{K}_\varepsilon \subseteq \mathbb{R}^d \setminus B$. Furthermore, observe that: since $L : \mathbb{R}^d \rightarrow |F(x) - \text{softmax} \circ \hat{F}(x)| \in \mathbb{R}$ is the composition of measurable and continuous functions then it, too is measurable; whence, $B \stackrel{\text{def}}{=} L^{-1}[[\varepsilon, \infty))$; must itself measurable.

Consequently, the following computations are well founded: Combining (10) and (11) we deduce that

$$\mathbb{P}\left(|F(X) - \text{softmax} \circ \hat{F}(X)| < \varepsilon\right) = \mu\left(|F(x) - \text{softmax} \circ \hat{F}(x)| < \varepsilon\right) \quad (12)$$

$$\begin{aligned} &= \mu(\mathbb{R}^d \setminus B) \\ &\geq \mu(\mathcal{K}_\varepsilon) \\ &\geq 1 - \varepsilon. \end{aligned} \quad (13)$$

Finally, by Proposition 1.1 and (1), we know that

$$F(X) = f(X, Z). \quad (14)$$

Whence, incorporating the identity in (14) into the left-hand side of the chain of inequalities in (12)-(13) implies that

$$\mathbb{P}\left(|f(X, Z) - \text{softmax} \circ \hat{F}(X)| < \varepsilon\right) = \mathbb{P}\left(|F(X) - \text{softmax} \circ \hat{F}(X)| < \varepsilon\right) \geq 1 - \varepsilon \quad (15)$$

which concludes our proof. \square